Sensitivity Analysis and Parameter Tuning Scheme for Global Sea-Ice Modeling

Jong G. Kim[a], Elizabeth C. Hunke[b], and
William H. Lipscomb[b]

[a]*MCS Division, Argonne National Laboratory, Argonne, Illinois USA*

[b]*MS-B216 Theoretical Division, Los Alamos National Laboratory, Los Alamos, New Mexico USA*

Abstract

Automatic differentiation (AD) is used to perform a multiple parameter sensitivity analysis for the Los Alamos sea-ice model CICE. Numerical experiments are run by six-hourly, 1997 forcing data with a two-hour time step, and the AD-based sensitivity scheme is validated by comparison with derivatives calculated using the conventional finite-difference approach. Twenty-two thermodynamic and dynamic parameters are selected for simultaneous analysis. Of these, the most important for controlling the simulated average sea-ice thickness is ice density; albedos and emissivity predominate in summer, while ice thickness is most sensitive to the ice conductivity in winter. The ice-ocean drag parameter and maximum ice salinity significantly affect the simulation year-round. Gradient information computed by the AD-based sea-ice code is then used in an experiment designed to assess the efficacy of this technique for tuning the parameters against observational data. Preliminary results, obtained with a bound-constrained minimization method and with simulated observational data, show that satisfactory convergence is obtained.

Key words: sea-ice model, automatic differentiation, parameter sensitivity, ice thickness, thermodynamics, dynamics, Arctic, Antarctic, Weddell Sea

1 Introduction

Seasonal sea-ice changes in the polar regions play an important role in the global climate system. Sea ice in the Arctic and Antarctic acts as a power-

Email addresses: `jgkim@mcs.anl.gov` (Jong G. Kim), `eclare@lanl.gov` (Elizabeth C. Hunke), `lipscomb@lanl.gov` (William H. Lipscomb).

ful insulating boundary layer, reducing the atmosphere-ocean heat exchange and reflecting incoming solar radiation. In greenhouse gas response experiments, researchers have observed enhanced warming caused by the thinning and complete disappearance of sea ice (Holland and Bitz, 2003).

Various thermodynamic and dynamic models have been developed to understand the physical mechanisms of sea ice and their role in global climate. Models provide useful information about sea-ice variables such as ice thickness, concentration, and horizontal velocity. Vertical ice growth rates are computed based on a thermodynamic energy balance that depends on ice temperature and on atmosphere and ocean forcing. The ice velocity is computed by integrating a two-dimensional momentum balance equation and then is used to determine ice transport and ridging.

These models include a number of thermodynamic and dynamic parameters that introduce substantial uncertainty. Rothrock et al. (2003) compiled published ice thickness predictions from eight different models for the period 1987–1997 and found large discrepancies among the results. To assess the possible impact of model parameters on simulation results, researchers have conducted a broad range of parametric sensitivity studies. Early sensitivity studies include the works of Maykut and Untersteiner (1971) and Semtner (1976) using one-dimensional, thermodynamic sea-ice models. Other researchers have coupled sea-ice dynamics with a thermodynamic model and carried out sensitivity analyses (Parkinson and Washington, 1979; Holland et al., 1993; Chapman et al., 1994; Harder and Fischer, 1999; Kreyscher et al., 2000; Miller et al., 2005). Parametizations range widely, covering numerical algorithms, physical sea-ice processes, and various implementations for surface forcing by the atmosphere and ocean. Specific parameters usually include atmosphere and ocean drag coefficients, an ice strength proportionality constant, and albedos, because these are believed to be the most influential for sea ice. Some studies incorporate a dozen or more parameters in various combinations (Holland et al., 1993; Chapman et al., 1994), requiring numerous simulations.

In recent work, Miller et al. (2005) optimized three sea-ice model parameters over the Arctic basin using CICE, the Los Alamos sea-ice model used here. They chose the atmospheric drag coefficient, the ice strength proportionality constant, and the cold, bare ice albedo. To obtain a unique triplet of optimized parameter values, they needed three sets of basin wide observations: Arctic ice extent, thickness, and velocity. They found that the resulting optimal values were interdependent—the optimal albedo depended on the ice strength constant, and so on. This study and the many earlier ones highlight two important points: the parameters need to be varied *simultaneously* to obtain optimal values, and identifying which parameters are most important for the simulation is not trivial.

In these previous experiments, sensitivity of a model variable such as thickness or velocity was not computed explicitly as a derivative of the variable with respect to the parameter, but rather was asessed by net change in the model solution. Sensitivities can be calculated by the finite difference (FD) method, which obtains derivatives by dividing the response perturbation by the input parameter variation, but truncation errors in this procedure can lead to erroneous derivatives. Furthermore, FD can be computationally costly because of the necessity of repeated runs. In this paper, we present an automatic differentiation (AD) technique as an alternative, which computes analytical derivatives within the sea-ice code. The AD code enables us to determine the sensitivities of the CICE model output variables to any given independent input parameters, simultaneously. Based on the AD-generated sensitivity data, we then develop a parameter-tuning scheme to maximize agreement between observed data and the simulation results. This study is intended to help climate modelers objectively identify important modeling parameters for designing optimized versions of sea-ice models.

Following a brief discussion of the model (Section 2) and the implementation scheme (Section 3), we discuss the numerical experiments used to evaluate the sensitivities (Section 4) and present the inverse modeling experiment. We conclude with a brief description of future work (Section 5).

2   Model Description

The major components of CICE are the thermodynamics, dynamics, and horizontal transport routines, which describe the physical state and motion of five ice thickness categories (each with four ice layers and one snow layer). The governing equations for each modeling component are solved on a generalized orthogonal grid by using an explicit time-step procedure. We summarize the main elements of the formulation here, identifying the parameters used in the numerical sensitivity experiments. A complete description of the sea-ice model used in this study, CICE version 3.1, can be found in Hunke and Lipscomb (2004).

2.1   Thermodynamic Parameters

In the thermodynamic portion of the model, an energy balance of radiative, turbulent, and conductive heat fluxes in each grid cell determines the temperature profile and thickness changes of ice and snow. The net energy flux from

3

the atmosphere to the ice (with all fluxes defined as positive downward) is

$$F_\circ = F_s + F_l + \epsilon F_{L\downarrow} + F_{L\uparrow} + (1 - \alpha)(1 - i_\circ)F_{sw}, \tag{1}$$

where F_s is the sensible heat flux, F_l is the latent heat flux, $F_{L\downarrow}$ is the incoming longwave flux, $F_{L\uparrow}$ is the outgoing longwave flux, F_{sw} is the incoming shortwave flux, α is the shortwave albedo, and $i_\circ$ is the fraction of absorbed shortwave flux that penetrates into the ice.

F_s, F_l, and $F_{L\uparrow}$ are functions of the ice surface temperature T_{sf}; Equation (1) is inverted to obtain T_{sf}. For instance, outgoing longwave radiation takes the standard blackbody form, $F_{L\uparrow} = -\epsilon\sigma\left(T_{sf}\right)^4$, where $\epsilon = 0.95$ (Briegleb, 1992) is the emissivity of snow or ice, σ is the Stefan-Boltzmann constant, and T_{sf} is the surface temperature in Kelvin. The sensible and latent heat fluxes are computed by using standard bulk formulas with a turbulence-based formulation for their exchange coefficients that depends on wind speed and stability of the atmospheric boundary layer. The minimum wind speed parameter, u_{min}, maintains finite sensible and latent heat fluxes when the wind is calm.

Total shortwave radiation impinging on the ice, F_{sw}, is divided three ways: a portion that is reflected, $-\alpha F_{sw}$; a portion that penetrates into the interior of the ice, $i_\circ(1 - \alpha)F_{sw}$; and the remainder that is absorbed at the ice or snow surface. The net absorbed flux, $(1 - \alpha)F_{sw}$, is actually a summation over two different radiative quantities (visible and near-infrared) for incoming shortwave with two corresponding albedos for each surface type (snow and ice). For $T_{sf} < -1°C$[1] and ice thickness $h_i > h_m = 0.5$ m, the standard bare ice albedo is $\alpha_{iv} = 0.78$ for visible wavelengths ($< 700\,\text{nm}$) and $\alpha_{in} = 0.36$ for near-infrared (IR) wavelengths ($> 700\,\text{nm}$). As h_i decreases from 0.5 m to zero, the ice albedo declines nonlinearly to the ocean albedo, 0.06. The ice albedo in both spectral bands decreases by 0.075 as T_{sf} rises from $-1°C$ to $0°C$. The albedo of cold snow ($T_{sf} < -1°C$) is $\alpha_{sv} = 0.98$ for visible wavelengths and $\alpha_{sn} = 0.70$ for near-IR wavelengths. The visible snow albedo decreases by 0.10 and the near-IR albedo by 0.15 as T_{sf} increases from $-1°C$ to $0°C$. Thus the albedo depends on the temperature and thickness of ice and snow as well as on the spectral distribution of the incoming solar radiation.

The flux of nonreflected shortwave radiation penetrating into the ice is $I_\circ = i_\circ(1 - \alpha)F_{sw}$, where $i_\circ = i_c(1 - f_{snow})$ and $i_c = 0.70$ for visible radiation and 0 for near-IR radiation. The snow area fraction f_{snow} depends on the snow depth, ranging from zero where there is no snow to near 1 for very deep snow. Radiation penetrating into the ice is attenuated according to Beer's law:

$$I(z) = I_\circ \exp(-\kappa_i z), \tag{2}$$

---

[1] This value is $-5°C$ in CICE version 3.0.1 used by Miller et al. (2005).

where $I(z)$ is the shortwave flux that reaches depth z beneath the surface without being absorbed and κ_i is the bulk extinction coefficient for solar radiation in ice, set to 1.4 m^{-1} for visible wavelengths (Ebert et al., 1995). A fraction $\exp(-\kappa_i h_i)$ of the penetrating solar radiation passes all the way through the ice to the ocean.

The rate of temperature change in the ice interior is given by Maykut and Untersteiner (1971):

$$\rho_i c_i \frac{\partial T_i}{\partial t} = \frac{\partial}{\partial z}\left(k_i \frac{\partial T_i}{\partial z}\right) - \frac{\partial I}{\partial z}, \tag{3}$$

where $\rho_i = 917$ kg/m^3 is the sea-ice density (assumed to be uniform), c_i is the specific heat of sea ice, k_i is the thermal conductivity of sea ice, and z is the vertical coordinate, defined to be positive downward with $z = 0$ at the top surface.

Following Untersteiner (1964), the thermal conductivity is given by

$$k_i(T, S) = k_\circ + \frac{\beta S}{T}, \tag{4}$$

where $k_\circ = 2.03$ W/m/deg is the conductivity of fresh ice, $\beta = 0.13$ W/m/psu is an empirical constant, S is the ice salinity, and the temperature T is in °C in this formula. The specific heat of sea ice also depends on both T and S.

The corresponding equation for the temperature change in snow is

$$\rho_s c_s \frac{\partial T_s}{\partial t} = \frac{\partial}{\partial z}\left(k_s \frac{\partial T_s}{\partial z}\right), \tag{5}$$

where $\rho_s = 330$ kg/m^3 is the snow density (assumed uniform), c_s is the specific heat of snow, and $k_s = 0.30$ W/m/deg is the thermal conductivity of snow. Penetrating solar radiation is neglected in (5) because most of the incoming sunlight is absorbed near the top surface when snow is present.

The salinity profile varies from $S = 0$ at the top surface ($z = 0$) to $S = S_{max}$ at the bottom surface ($z = 1$) and is similar to that used by Maykut and Untersteiner (1971).

An equation similar to (1) applies at the bottom of the ice. The net downward heat flux from the ice to the ocean is given by Maykut and McPhee (1995):

$$F_{bot} = -\rho_w c_w c_h u_*(T_w - T_f), \tag{6}$$

where ρ_w is the density of seawater, c_w is the specific heat of seawater, $c_h = 0.006$ is a heat transfer coefficient, T_w is the sea surface temperature, T_f is the salinity-dependent freezing temperature, and $u_* = \sqrt{|\vec{\tau}_w| / \rho_w}$ is the friction velocity used under melting conditions. Under freezing conditions, F_{bot} represents a potential to freeze ice, with $c_h u_*$ replaced by $h_{mix}/\Delta t$. Here, h_{mix} is the mixed layer depth, and Δt is the model time step.

Ablation or accretion at the bottom of the ice is given by

$$\frac{\partial h}{\partial t} = \frac{F_{cond} - F_{bot}}{q}, \tag{7}$$

where

$$q = -\rho_i \left[c_\circ \left(T_m - T \right) + L_\circ \left(1 - \frac{T_m}{T} \right) - c_w T_m \right] < 0, \tag{8}$$

$c_\circ$ is the specific heat of fresh ice, $L_\circ$ is the latent heat of fusion of fresh ice, and T_m is the salinity-dependent melting temperature. A similar relation holds for melting at the top of the ice or snow.

2.2   Dynamics and Ridging Parameters

Ice motion and deformation are determined by balancing five major stresses: wind stress from the atmosphere, water stress from the interaction between ice and ocean, Coriolis force, the stress from the tilt of the ocean surface, and the internal ice stress. A momentum balance equation is solved to obtain the ice velocity in each grid cell, using the elastic-viscous-plastic (EVP) rheology (Hunke and Dukowicz, 2002) to relate the internal ice stress and the rates of strain. The ice strength (or pressure, P) is determined by an energy-based ridging scheme (Rothrock, 1975; Hibler, 1980) and used in the EVP ice dynamics component to compute the internal ice stress.

The surface layer currents, $\vec{U}_w$, are used to determine the stress between the ocean and the ice. This stress takes the form

$$\vec{\tau}_w = c_w \rho_w \left| \vec{U}_w - \vec{u} \right| \left(\vec{U}_w - \vec{u} \right). \tag{9}$$

In the sensitivity experiments below, $c_w \rho_w$ is treated as a single parameter, D_w.

The elastic modulus is defined in terms of a damping timescale T for elastic waves such that $T = E_\circ \Delta t$; $E_\circ$ is a tunable parameter less than one.

Along with the velocity field, we compute the strain rates, or deformation, of the ice. Ice divergence and convergence cause the ice to ridge (we use "ridging" as shorthand for all forms of mechanical redistribution). Thin ice is converted to thick, ridged ice in a way that reduces the total ice area while conserving ice volume and internal energy. A weighting function $b(h)$ favors ridging of thin ice and closing of open water in preference to ridging of thicker ice. Following Thorndike et al. (1975), we set

$$b(h) = \begin{cases} \frac{2}{G^*}(1 - \frac{G(h)}{G^*}) & \text{if } G(h) < G^* \\ 0 & \text{otherwise,} \end{cases} \tag{10}$$

where $G(h)$ is the fractional area covered by ice thinner than h and where G^* is an empirical constant. If the open water fraction is greater than G^*, no ice can ridge because ridging simply reduces the area of open water. As in Thorndike et al. (1975) we set $G^* = 0.15$.

Following Hibler (1980), ridging ice of thickness h forms ridges whose area is distributed uniformly between $H_{\min} = 2h$ and $H_{\max} = 2\sqrt{H^*h}$. The default value of H^* in CICE is 25 m, although it is taken to be 100 m in other models (Flato and Hibler, 1995; Bitz et al., 2001; Briegleb et al., 2004). This ridged ice distribution effectively causes the ice strength to scale as $P \sim h^{3/2}$. Larger values of G^* allow thicker ice to participate in ridging, thereby increasing the ice strength.

C_s is the fraction of shear dissipation energy that contributes to ridge building. Another empirical parameter, C_f, accounts for frictional energy dissipation. Following Flato and Hibler (1995), we set $C_s = 0.25$ and $C_f = 17$. Finally, when ice ridges, a fraction of the snow is thrown into the ocean, while the rest, F_{srdg}, remains on top of the ridged ice.

2.3   Unavailable Parameters

Most previous parameter sensitivity analyses for sea-ice models have included an air-ice drag coefficient and an ice strength proportionality constant (universally notated P^* following Hibler (1979)), including the study by Miller et al. (2005) using an older version of CICE. These parameters are not used in the current version of CICE. We use the energetics-based ice strength formulation described above, which closely corresponds with our ridging scheme, rather than the simpler, empirical ice strength parameterization of Hibler (1979).

Likewise, rather than specifying a constant air-ice drag coefficient, CICE computes a variable drag coefficient whose value depends on the stability of the

Table 1
Model parameters chosen for sensitivity testing via automatic differentiation, listed in the order in which they appear in the text.

Parameter	Description	Value
Thermodynamic Parameters		
ϵ	emissivity of snow and ice	0.95
u_{min}	minimum wind speed for turbulent fluxes	1 m/s
α_{iv}	visible ice albedo	0.78
α_{in}	near-IR ice albedo	0.36
α_{sv}	visible cold snow albedo	0.98
α_{sn}	near-IR snow albedo	0.70
i_c	penetrating fraction of visible solar radiation	0.7
κ_i	visible extinction coefficient in ice	1.4 m^{-1}
ρ_i	ice density	917 kg/m^3
β	T, S proportionality constant in conductivity	0.13 W/m/psu
$k_{\circ}$	thermal conductivity of fresh ice	2.03 W/m/deg
ρ_s	snow density	330 kg/m^3
k_s	thermal conductivity of snow	0.30 W/m/deg
S_{max}	maximum salinity, at ice base	3.2 psu
h_{mix}	ocean mixed-layer depth	20 m
Dynamic Parameters		
D_w	drag parameter for water on ice	0.00536 * 1026 kg/m^3
$E_{\circ}$	ratio of damping time scale to time step	0.36
G^*	fractional area participating in ridging	0.15
H^*	determines mean thickness of ridged ice	25 m
C_s	fraction of shear energy contributing to ridging	0.25
C_f	ratio of ridging work to PE change in ridging	17.
F_{srdg}	snow fraction that survives in ridging	0.5

atmosphere. Stössel (1992) found that including the stability dependence improved his results. Analogous, parallel formulations are used to determine turbulent exchange coefficients for latent and sensible heat fluxes simultaneously with the air-ice drag coefficient. There are nearly 20 parameters in the atmospheric boundary layer description alone, although many are well constrained by observations. We include only one parameter (u_{min}) from this parameterization in the sensitivity analysis discussed below. Our chosen parameters, listed in Table 1, pertain primarily to the ice physics and associated numerical formulations rather than to the forcing; however, such a line is not easily drawn.

3　AD-based Implementation Scheme

Automatic differentiation is an alternative to the conventional FD method for model sensitivity analysis. AD relies on the fact that the derivatives of a function, no matter how complicated, can be computed by repeatedly applying the chain rule of derivative calculus to the sequential elementary operations of a coded function. For example, if a function f is computed through the elementary functional operations $y(x)$ and $z(x)$, the chain rule can be applied to compute the partial derivative of f with respect to the independent variable x as follows:

$$\frac{\partial f(y,z)}{\partial x} = \frac{\partial f}{\partial y}\frac{\partial y}{\partial x} + \frac{\partial f}{\partial z}\frac{\partial z}{\partial x}, \tag{11}$$

By applying the chain rule repeatedly, we can compute analytical derivatives of any computational function, because the computer code representing the function is the composite of elementary operations. Note that AD allows augmenting any computer program written in Fortran, C, or C^{++} for derivative computations (Bischof et al., 1996).

Various implementation techniques for AD processing have been developed. Juedes (1991) provides an extensive survey of available AD tools. The two basic implementation approaches are referred to as the forward and reverse modes. In the forward mode, derivatives of intermediate functional values are computed with respect to the input primary parameters. It is known from the linearity of differentiation that the computational effort required in this mode is approximately dependent on the number of input parameters multiplied by the runtime and memory of the original program.

In the reverse mode, AD propagates derivatives of the final result with respect to intermediate quantities known as adjoints. The program flow is reversed in order to be able to keep all of the adjoints that affect the final result. Because intermediate values must be stored or recomputed, however it is difficult to estimate the storage requirement using the reverse mode. Recent AD research has therefore centered on hybrid modes, which combine the best features of the forward and reverse modes.

In this study, we use the ADIFOR tool (Bischof et al., 1996) developed by Argonne National Laboratory and Rice University, which employs a hybrid forward/reverse mode approach to generate derivatives. Given a function computation in Fortran and a control description of which variables correspond to independent and dependent parameters, ADIFOR produces portable Fortran code that computes the partial derivatives of the dependent variables with respect to the independent variables.

The ADIFOR product code can be linked with a minimization algorithm for determining the optimal sea-ice model parameters, thus providing accurately tuned parameters based on observational data. In this study, a quasi-Newton method was tested for its ability to optimize model parameters. This method, the limited-memory Broyden-Fletcher-Goldfarb-Shanno algorithm (L-BFGS-B), is described by Zhu et al. (1994). To avoid numerically unstable simulation results, we initially constrain each parameter to an acceptable range. The objective function (or cost function) and its gradient information required by the L-BFGS-B algorithm are provided by the ADIFOR-processed CICE code. We test the convergence of this formulation using simulated ice thickness data, in preparation for tuning the parameters with thickness data based on observations.

Automatic differentiation techniques have been used to analyze parameter sensitivities in atmosphere and ocean models (Park and Droegemeier, 1999; Slawig and Zickfeld, 2004; Kioutsioukis et al., 2005; Sandu et al., 2005). In the following section, we present the results of our sensitivity analysis and proof of concept for our parameter-tuning implementation. To our knowledge, this is the first simultaneous parameter sensitivity analysis performed on a sea-ice model using automatic differentiation.

4 Numerical Results

4.1 Experiment Design

The CICE model experiments discussed below are performed on a coarse global grid (3°) that includes both polar regions. Atmospheric forcing fields for 1997 are interpolated to the two-hour time step. This data includes six-hourly, 10 m data for air temperature, air density, specific humidity, and wind velocity from the National Centers for Environmental Prediction (NCEP) reanalyses (Kalnay et al., 1996), International Satellite Cloud Climatology Project (ISCCP) (Rossow and Schiffer, 1991) monthly downward shortwave radiation flux and cloud fraction, and monthly precipitation fields (MSU) (Spencer, 1993). The model is initialized with a 35-year spin-up using the 1997 forcing data. The resulting ice thickness, concentration, and velocity fields on January 1 are used as the initial state for the experiments described in the following subsections.
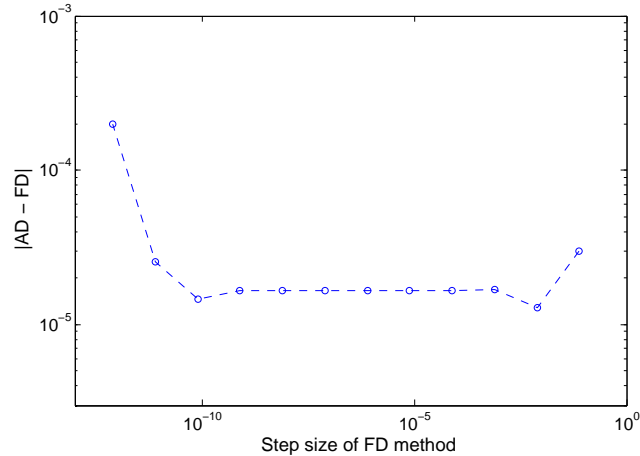
Fig. 1. Comparison of AD and FD derivates for different FD step sizes ($\Delta\alpha_{iv}$).

4.2 Validation

The AD-augmented CICE code was validated by comparing the AD-computed derivatives with the finite difference results, differentiating the ice thickness in central Arctic with respect to the visible ice albedo α_{iv} after one week. Differences between the AD and FD derivatives are summarized in Fig. 1 for various step sizes used to compute the FD derivatives. Numerical errors in the FD derivatives, particularly for small step sizes, are associated with truncation of the Taylor expansion and cancellation in subtraction of very small floating-point numbers. Truncation in the AD derivative calculation is eliminated because all the partial derivatives of elementary functional operations can be computed analytically. Good agreement between the AD and FD results over a large range of step sizes indicates that the AD approach using ADIFOR is working correctly for the CICE model code.

4.3 AD Sensitivity Experiment

The sensitivity experiment is carried out with respect to a primary dependent variable, average ice thickness (or more precisely, ice volume per unit area), at three locations: the central Arctic (90 N), Fram Strait (79 N, 6 W), and Weddell Sea (70 S, 40 W). Based on the dynamic and thermodynamic ice model described in Section 2, 22 parameters were identified for testing. Table 1 lists these independent variables with the standard values used in CICE.

The results of the AD sensitivity experiment are summarized in Figs. 2–4 and Table 2. Derivatives (or "sensitivities") of the average ice thickness at three
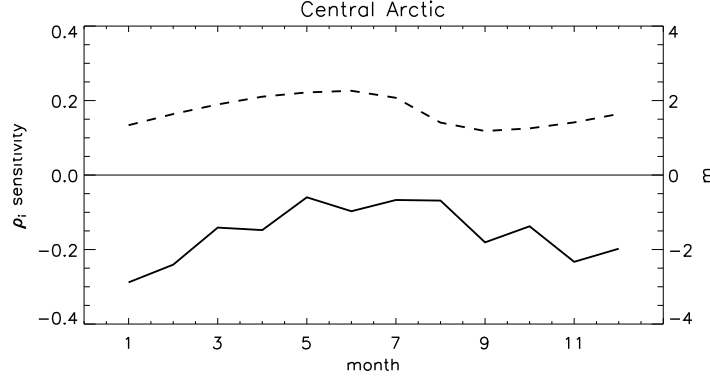
11

Fig. 2. Time series of ice thickness (right axis, m) and nondimensionalized ice density sensitivity (left axis).

different locations, with respect to each of the test parameters, were calculated by using the AD-processed code and then were nondimensionalized by using the average thickness for the analysis time period (Fig. 2) and the standard parameter values. That is, Table 2 and Figs. 2–4 give

$$\frac{p}{\bar{h}} \frac{\partial h}{\partial p}$$

for parameters p. Table 2 lists 12-month sums of sensitivity magnitudes for each of the 22 parameters, with larger values indicating greater sensitivity. Figure 2 illustrates the seasonal variability of the parameter sensitivity with the greatest values, the ice density ρ_i, and Figs. 3–4 show time series for the remaining parameters whose sum over all months and all three grid points are greatest. Each individual value represents an average over the first week of the month. The sums in Table 2 are of the magnitudes of the derivatives and thus are proportional to the total area under the timeseries curves in Figs. 2–4.

Ice density dominates the sensitivity analysis, but this sensitivity is largely an artifact of the way density is treated in the code. The model state variables are area A, volume V, and internal energy e, with thickness h and enthalpy q diagnosed as V/A and e/V, respectively. Temperature T is diagnosed from q by using (8). Thus, an initial increase in ρ_i for a given q is associated with a smaller value of the specific heat of melting (the bracketed term on the right-nad side of Eq. 8) and a higher temperature. This unphysical warming reduces winter ice growth and, to a lesser extent, increases summer melting. It is necessary to run the model for several years with a modified ρ_i to determine the true sensitivity of the thickness to ice density. Such an experiment is discussed in the next section.

The other parameters produce more intuitive results (Figs. 3–4). For instance, in the summer months (July–September in the central Arctic, December–February in the Weddell Sea, June in Fram Strait before the grid cell becomes
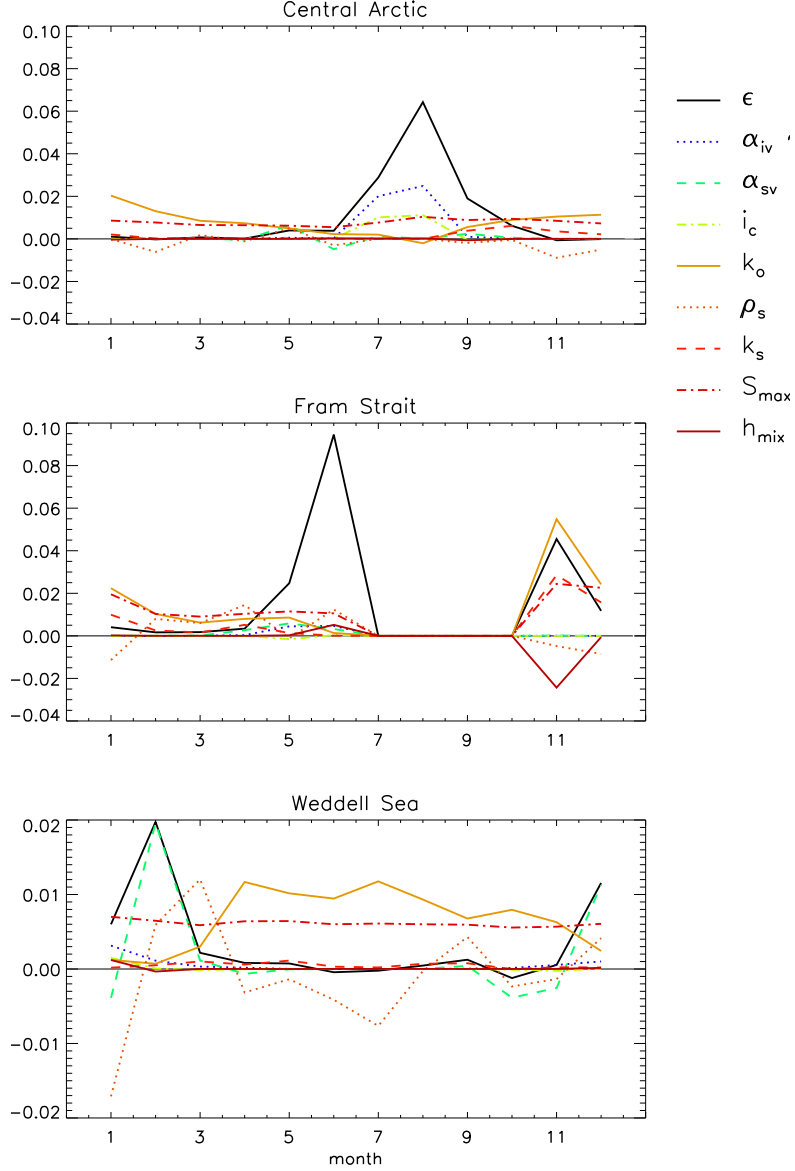
12

Fig. 3. Time series of nondimensionalized AD derivatives, for the 11 most important thermodynamic parameters from Table 2. Parameters are listed in decreasing order of importance (averaged over all months and the 3 grid points) in the legend; α_{in} and α_{sn} sensitivities are slightly less than those for α_{iv} and α_{sv}, respectively, but are not different enough to warrant plotting separately. Time series of the remaining thermodynamic parameters are not distinguishable from zero here. The grid cell in Fram Strait is essentially ice-free July–October; because zero thicknesses cause the nondimensionalized sensitivity values to be infinite, we have set them to zero.

ice-free), radiative parameters play the greatest role in determining the ice volume. Emissivity ϵ is the most important radiative parameter overall, reflecting the importance of net longwave, $F_{net} = \epsilon \left(F_{L\downarrow} - \sigma T_{sf}^4 \right)$, in the surface flux balance of Eq. 1. Increasing ϵ increases the negative magnitude of F_{net} (positive downward), thus cooling and thickening the ice.
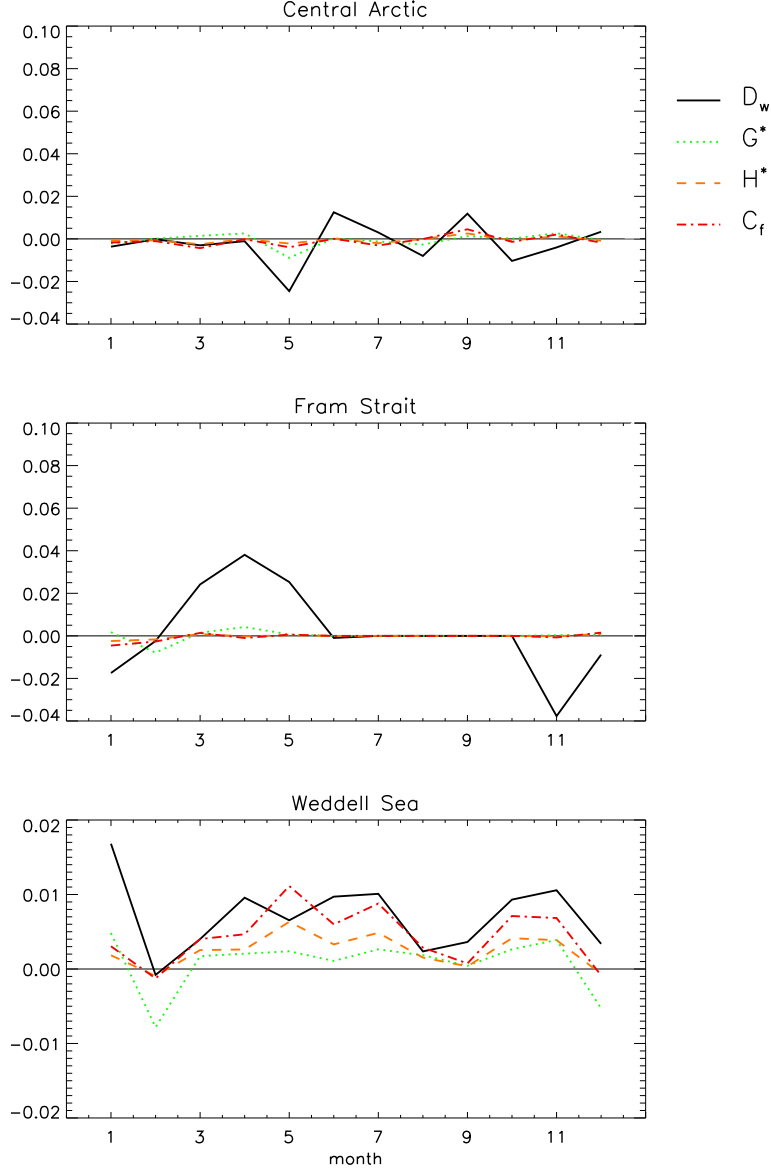
Fig. 4. As in Fig. 3, for the 4 most important dynamics parameters from Table 2.

Albedos vie for importance based on the strength of solar radiation. Visible and near-IR snow albedos (α_{sv} and α_{sn}) are prominent in spring in the central Arctic, when the ice is still snow-covered, but by later in the summer the ice albedos α_{in} and α_{iv} predominate. The fraction of visible solar radiation that penetrates into the ice also influences the ice volume during central Arctic summer months. Snow albedos prevail over ice albedos in the Weddell Sea, reflecting the fact that ice in the region remains snow-covered throughout the summer. Ice thickness in the Weddell Sea is also less sensitive to emissivity than is Northern Hemisphere sea ice.

The most influential parameters in winter are snow and ice conductivities and S_{max}, the maximum salinity, which also affects the ice conductivity (Eq. 4)

14

Table 2
Magnitudes of AD sensitivities, summed over the 12 months for each test point. The "Total" column gives the sum over 12 months and all three points; time series of the parameters with largest total values are shown in Fig. 3–4.

Parameter	Central Arctic	Fram Strait	Weddell Sea	Total
Thermodynamic Parameters				
ϵ	1.2886E-01	1.8745E-01	4.5160E-02	3.6147E-01
u_{min}	4.7376E-04	3.1519E-04	5.0220E-04	1.2911E-03
α_{iv}	4.6819E-02	9.5705E-03	6.4883E-03	6.2878E-02
α_{in}	4.2833E-02	3.2537E-03	3.1728E-03	4.9259E-02
α_{sv}	1.5922E-02	1.2030E-02	4.3442E-02	7.1394E-02
α_{sn}	9.7470E-03	4.0040E-03	2.9042E-02	4.2793E-02
i_c	2.1975E-02	1.9268E-03	2.1338E-03	2.6035E-02
κ_i	4.1383E-03	5.4852E-04	1.9862E-04	4.8854E-03
ρ_i	1.8593E+00	2.0759E+00	1.8791E+00	5.8144E+00
β	6.0095E-03	8.0442E-03	4.9687E-03	1.9022E-02
$k_\circ$	9.6795E-02	1.3585E-01	8.0720E-02	3.1337E-01
ρ_s	3.3574E-02	6.6670E-02	6.3792E-02	1.6404E-01
k_s	1.8908E-02	6.4876E-02	5.8382E-03	8.9622E-02
S_{max}	9.3055E-02	1.1834E-01	7.3554E-02	2.8495E-01
h_{mix}	1.8141E-03	3.0620E-02	1.7654E-03	3.4199E-02
Dynamic Parameters				
D_w	8.5642E-02	1.5489E-01	8.6769E-02	3.2730E-01
$E_\circ$	4.3678E-04	4.2895E-04	2.9319E-04	1.1589E-03
G^*	2.3963E-02	1.6827E-02	3.6584E-02	7.7375E-02
H^*	1.3703E-02	6.5809E-03	3.2946E-02	5.3230E-02
C_s	1.3379E-03	2.0138E-03	8.0453E-04	4.1561E-03
C_f	2.4109E-02	1.2392E-02	5.7342E-02	9.3843E-02
F_{srdg}	4.9359E-04	1.3721E-03	1.0408E-03	2.9065E-03

and melting or freezing at the ice-ocean interface. When the conductivity is larger, heat is more readily transferred upward through the ice, allowing faster growth at the bottom surface. S_{max} plays a prominent role year-round, in all three regions, with a moderate sensitivity of 0.01.

Four of the dynamics parameters are listed among the 15 most influential parameters; except for the ocean drag parameter, all have sensitivities of 0.01 or less. The drag coefficient is another parameter that is important all year, with sensitivity magnitudes among the highest of this 22-parameter set (it is third most influential, following ρ_i and ϵ). This result corroborates the parameter selections of numerous previous sensitivity studies. Our only parameter related to the atmosphere-ice drag coefficient, u_{min}, places very low. Likewise,

the least important dynamics parameters are the EVP parameter $E_\circ$ and two parameters related to the ridging scheme, F_{srdg} and C_s (Table 2).

It is heartening that many of the parameters lacking strong physical constraints are relatively unimportant to the model's physical solution. For instance, the addition of elastic waves to the viscous-plastic rheology was intended only as a numerical artifice for making the code more efficient; thus we would not expect $E_\circ$ to significantly affect the solution. Among thermodynamic parameters in this sensitivity study, the least important overall are β, the salinity/temperature proportionality constant in the formula for ice conductivity (Eq. 4), the extinction coefficient κ_i, and the minimum wind speed used to compute turbulent fluxes over the ice and snow, u_{min}.

From this analysis we see that parameters affecting the conductivity and radiative absorption are of paramount importance for simulating ice volume in the sea-ice model; with the exception of D_w, dynamics and ridging parameters are less important than the thermodynamic parameters. If we were using ice velocity as the dependent variable, however, the dynamics parameters would be more prominent.

4.4   Single Parameteric Sensitivities

We have also assessed the model's robustness to individual modeling parameters. Several of these single-parametric sensitivity results are shown in Fig. 5, for the central Arctic. For instance, Fig. 5a and b demonstrate that increasing (decreasing) the ice albedo or conductivity results in thicker (thinner) ice.

Figure 5 also illustrates how a long-term simulation may exhibit unexpected sensitivity to parameters such as ice and snow density, which may not be reflected in the AD sensitivities. For instance, decreased ice density increases the ice thickness during the first two winters of the simulation. However, an eventual decrease of ice thickness is observed as the simulation continues over five years, associated with increasing summer melt that eventually dominates ice growth in winter. A decrease in the snow density that initially produces little response in ice thickness leads to decreased ice thickness after the first summer. The magnitude of the change by year 5 is comparable to the change given by the ice density.

4.5   Parameter Tuning Proof of Concept

As described in Section 2, the sea-ice model relies strongly on the interplay between dynamic and thermodynamic processes. While it is possible to obtain
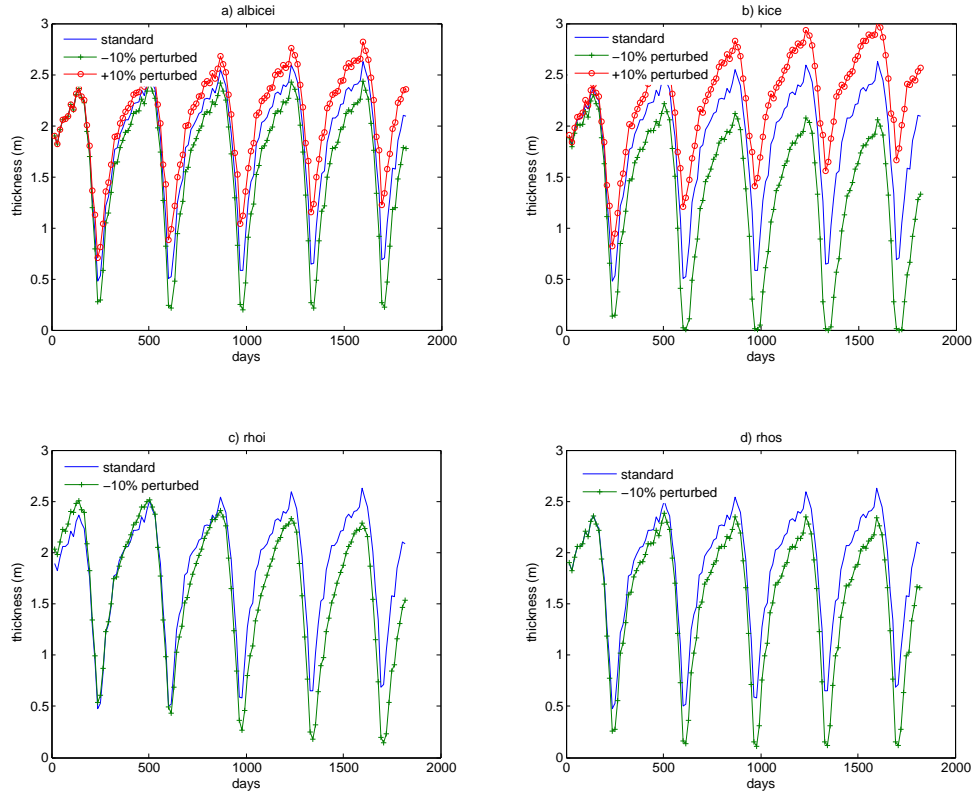
Fig. 5. Single-parameteric sensitivity results for five-year runs with standard and perturbed parameter values. (a) near-IR ice albedo, α_{in}, (b) fresh ice conductivity, $k_\circ$, (c) ice density, ρ_i, (d) snow density, ρ_s.

realistic values of one field through compensating errors, it is difficult to obtain realistic values of all variables at all grid points. Optimal model parameters can be obtained, however, given sufficient, accurate observations. By "sufficient" we refer to the number of degrees of freedom available in the observations; no more parameters may be optimized than the degrees of freedom in the observational data. Here we demonstrate that AD parameter optimization methods can be successfully applied to the CICE code.

The parameter-tuning process couples the derivative code generated by ADI-FOR with a quasi-Newton minimization code. We used the bound-constrained, limited-memory BFGS method, which minimizes a nonlinear function of n variables subject to lower and upper bounds on the variables. The derivatives of the cost function are computed by the AD-processed sea-ice modeling code and provided to the L-BFGS-B routine.

To test the viability of this approach, we first applied our technique to a simulated set of observation data: the model was run with known parameter values for $k_\circ$, ρ_i, and S_{max} for one week, and the simulation results of average ice thickness at the North Pole were stored as observations. We tested the
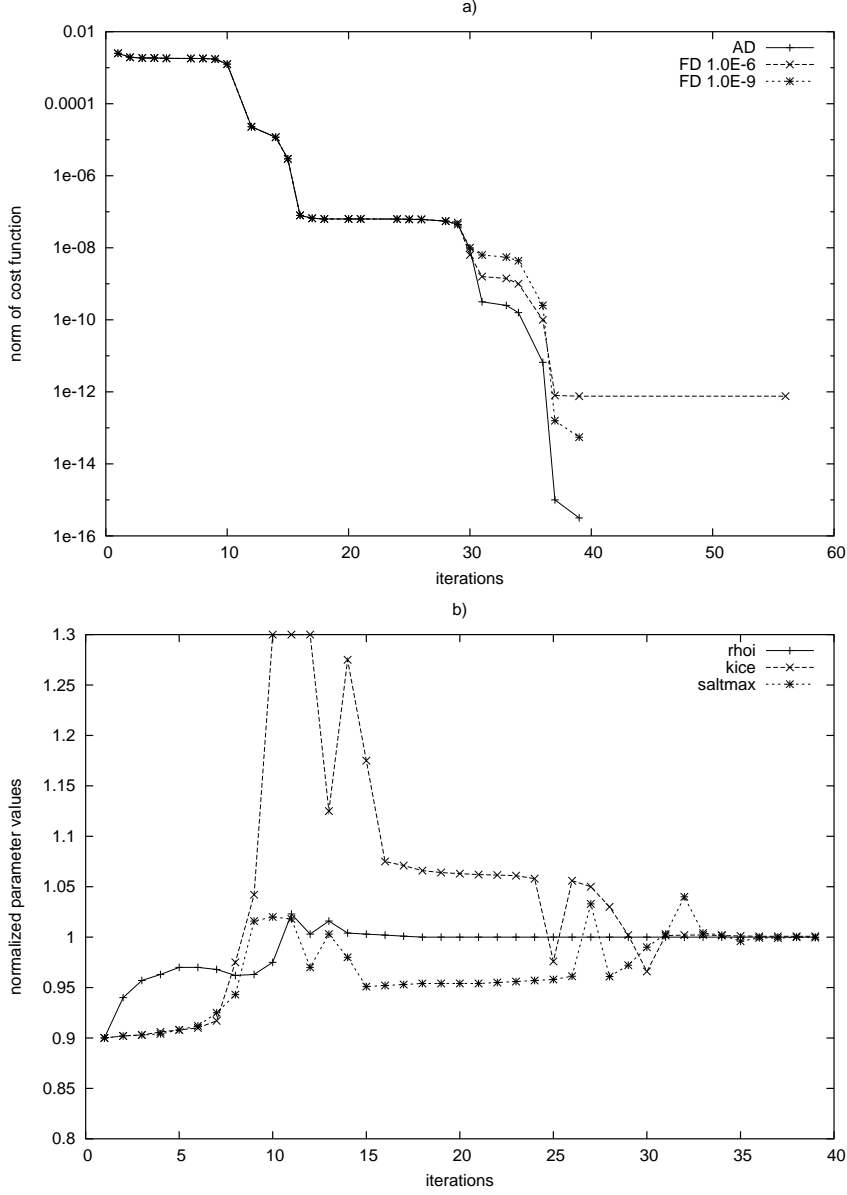
17

Fig. 6. Convergence behavior of (a) the optimization algorithm and (b) each of the parameters being tuned (parameter values are normalized). Two different step sizes were used for the FD tests in (a).

optimization method against this simulated observational data, using initial guesses for the three test parameters that were 10% smaller. Figure 6 shows the convergence behavior of the optimization algorithm and the convergence progress of each parameter in the optimization test. Upon convergence, the optimal parameter values are recovered to within three significant digits. Moreover, Fig. 6a indicates that AD-generated gradients provide faster convergence behavior in the tuning process than does the FD approach.

5 Discussion

For this study we choose average ice thickness, that is, the ice volume per unit area, as the dependent variable because it represents the integrated evolution of the ice pack through time and is critical for climate simulations, particularly for the fresh water balance of the climate system. Sea-ice concentration also plays a crucial role in Earth's energy budget because of the insulating and reflective properties of ice on the ocean surface; likewise, sea-ice velocity and associated deformation fields direct the pack-ice evolution. Although we consider only ice thickness in this paper, parameter sensitivites can be computed for concentration, velocity, or any of the model's prognostic variables.

By comparing automatic differentiation results with the FD method for differentiating ice thickness, we have verified that the AD technique provides an accurate sensitivity analysis of a multivariate sea-ice model, CICE. Overall, thermodynamic (radiative and conductivity) parameters strongly affect the ice-thickness simulation, and the ice-ocean drag coefficient also plays an important role.

Perhaps the most striking result from this study is the prominent sensitivity of ice thickness to emissivity ϵ. This parameter has not been scrutinized in sea-ice models. For instance, Ebert and Curry (1993) test the sensitivity of their one-dimensional sea-ice thermodynamics model to longwave forcing but do not vary the value of ϵ. Holland et al. (1993) consider ϵ in their set of sensitivity runs but do not discuss their results. Our standard value of 0.95 is somewhat lower than that typically used in models, 0.97–0.99, but there is no general agreement on the best value. Furthermore, we use the same value for both ice and snow, while differing values are likely warranted. Observations made during the SHEBA program in the Arctic show significant variability in emissivity at microwave frequencies, with values often near 0.9 and below (Haggerty and Curry, 2001).

Model limitations likely contribute to under- or overestimates of sensitivities. Although CICE incorporates many recent advances in sea-ice modeling techniques, parameterizations, and algorithms, its snow model remains rather crude, with just one layer of snow and none of the more complex snow processes such as phase changes, densification, grain growth, and melt ponds. Parameter sensitivities in this model would probably change if the parameterizations were changed significantly; along the same lines, sensitivities in other models will likely be different.

Single-parameteric sensitivity experiments show that the model sensitivity is compounded during longer, multiple-year simulations and that feedback processes can change even the sign of the sensitivity. Thus, it is desirable to tune

19

the ice model by using an optimization process that simultaneously examines parameters in all of the model components. Miller et al. (2005) used large-scale observational data for Arctic ice thickness, concentration, and velocity to tune just three parameters, requiring 168 model runs. In our preliminary tests of the L-BFGS-B parameter-tuning algorithm, we find that the minimization algorithm converges quickly, yielding multiple model parameters that match those used to produce the simulated observational data, in just one run.

Our method presents difficulties of other sorts, however. We have found that spatially sparse data, such as buoy or ship-track data, can significantly worsen the sea-ice simulation, or even make it fail to converge. Furthermore, optimizing parameters based on different dependent variables (such as ice concentration or speed) may result in different parameter values. We expect that the data required to tune the model parameters will need to be consistent in time with the atmospheric forcing data that we apply to the model.

Miller et al. (2005) demonstrate that even with such difficulties, parameter optimization is possible. This study suggests which parameters should be tuned. In future work, we plan to further explore CICE's parameter space using the best available data for both hemispheres, including satellite-derived ice concentration and ice deformation. Furthermore, we plan to parallelize the CICE parameter-tuning algorithm using MPI protocols. This parallelization will allow us to tune the model using multidecadal and other long-term observational data, which should yield parameter estimates suitable for climate simulations.

Acknowledgment

References

Bischof, C., Carle, A., Khademi, P., Mauer, A., 1996. ADIFOR 2.0: Automatic differentiation of fortran 77 programs. IEEE Computational Science and Engineering 3(3), 18–32.

Bitz, C. M., Holland, M. M., Weaver, A. J., Eby, M., 2001. Simulating the ice-thickness distribution in a coupled climate model. J. Geophys. Res.–Oceans 106, 2441–2463.

Briegleb, B. P., 1992. Longwave band model for thermal radiation in climate studies. J. Geophys. Res. 97, 11,475–11,485.

Briegleb, B. P., Bitz, C. M., Hunke, E. C., Lipscomb, W. H., Holland, M. M., Schramm, J. L., Moritz, R. E., June 2004. Scientific description of the sea ice component in the Community Climate System Model, version 3. Technical Note TN-463+STR, National Center for Atmospheric Research.

Chapman, W. L., Welch, W. J., Bowman, K. P., Sacks, J., Walsh, J. E., 1994. Arctic sea ice variability: Model sensitivities and a multidecadal simulation. J. Geophys. Res.–Oceans 99, 919–935.

Ebert, E. E., Curry, J. A., 1993. An intermediate one-dimensional thermodynamic sea-ice model for investigating ice-atmosphere interactions. J. Geophys. Res.–Oceans 98, 10085–10109.

Ebert, E. E., Schramm, J. L., Curry, J. A., 1995. Disposition of solar radiation in sea ice and the upper ocean. J. Geophys. Res.–Oceans 100, 15,965–15,975.

Flato, G. M., Hibler, W. D., 1995. Ridging and strength in modeling the thickness distribution of Arctic sea ice. J. Geophys. Res.–Oceans 100, 18611–18626.

Haggerty, J. A., Curry, J. A., 2001. Variability of sea ice emissivity estimated from airborne passive microwave measurements during FIRE SHEBA. J. Geophys. Res. 106, 15,265–15,277.

Harder, M., Fischer, H., 1999. Sea ice dynamics in the Weddell Sea simulation with an optimized model. J. Geophys. Res. 104, 11,151–11,162.

Hibler, W. D., 1979. A dynamic thermodynamic sea ice model. J. Phys. Oceanogr. 9, 817–846.

Hibler, W. D., 1980. Modeling a variable thickness sea ice cover. Mon. Wea. Rev. 108, 1943–1973.

Holland, D. M., Mysak, L. A., Manak, D. K., Oberhuber, J. M., 1993. Sensitivity study of a dynamic thermodynamic sea ice model. J. Geophys. Res.–Oceans 98, 2561–2586.

Holland, M. M., Bitz, C. M., 2003. Polar amplification of climate change in coupled models. Climate Dyn. 21, 221–232.

Hunke, E. C., Dukowicz, J. K., 2002. The Elastic-Viscous-Plastic sea ice dynamics model in general orthogonal curvilinear coordinates on a sphere—Effect of metric terms. Mon. Wea. Rev. 130, 1848–1865.

Hunke, E. C., Lipscomb, W. H., 2004. CICE: the Los Alamos Sea Ice Model, Documentation and Software, version 3.1. Tech. Rep. LA-CC-98-16, Los Alamos National Laboratory, Los Alamos, New Mexico.
URL http://climate.lanl.gov/Models/CICE

Juedes, D., 1991. A taxonomy of automatic differentiation tools. In: Griewank, A., Corliss, G. (Eds.), Proceedings of the Workshop on Automatic Differentiation of Algorithms: Theory, Implementation, and Application. Society for Industrial and Applied Mathematics, Philadelphia, pp. 315–330.

Kalnay, E., Kanamitsu, M., Kistler, R., Collins, W., Deaven, D., Gandin, L., Iredell, M., Saha, S., White, G., Woollen, J., Zhu, Y., Chelliah, M., Ebisuzaki, W., Higgins, W., Janowiak, J., Mo, K. C., Ropelewski, C.,

Wang, J., Leetmaa, A., Reynolds, R., Jenne, R., Joseph, D., 1996. The NCEP/NCAR 40-year reanalysis project. Bull. Amer. Meteor. Soc. 77, 437–471.

Kioutsioukis, I., Melas, D., Zerefos, C., Ziomas, I., 2005. Efficient sensitivity computations in 3D air quality models. Comp. Phys. Comm. 167, 23–33.

Kreyscher, M., Harder, M., Lemke, P., Flato, G. M., 2000. Results of the Sea Ice Model Intercomparison Project: Evaluation of sea ice rheology schemes for use in climate simulations. J. Geophys. Res. 105, 11,299–11,320.

Maykut, G. A., McPhee, M. G., 1995. Solar heating of the Arctic mixed layer. J. Geophys. Res.–Oceans 100, 24691–24703.

Maykut, G. A., Untersteiner, N., 1971. Some results from a time dependent thermodynamic model of sea ice. J. Geophys. Res. 76, 1550–1575.

Miller, P. A., Laxon, S. W., Feltham, D. L., Cresswell, D. J., 2005. Optimization of a sea ice model using basin-wide observations of Arctic sea ice thickness, extent and velocity. J. Clim., in press.

Park, S. K., Droegemeier, K. K., 1999. Sensitivity analysis of a moist 1D Eulerian cloud model using automatic differentiation. Mon. Wea. Rev. 127, 2180–2196.

Parkinson, C. L., Washington, W. M., 1979. A large-scale numerical model of sea ice. J. Geophys. Res. 84, 311–337.

Rossow, W. B., Schiffer, R. A., 1991. ISCCP cloud data products. Bull. Amer. Meteor. Soc. 72, 2–20.

Rothrock, D. A., 1975. The energetics of the plastic deformation of pack ice by ridging. J. Geophys. Res. 80, 4514–4519.

Rothrock, D. A., Zhang, J., Yu, Y., 2003. The arctic ice thickness anomaly of the 1990s: A consistent view from observations and models. J. Geophys. Res.–Oceans 108(C3), 3083, doi:10.1029/2001JC001208.

Sandu, A., Daescu, D. N., Carmichael, G. R., Chai, T. F., 2005. Adjoint sensitivity analysis of regional air quality models. J. Comp. Phys. 204, 222–252.

Semtner, A. J., 1976. A model for the thermodynamic growth of sea ice in numerical investigations of climate. J. Phys. Oceanogr. 6, 379–389.

Slawig, T., Zickfeld, K., 2004. Parameter optimization using algorithmic differentiation in a reduced-form model of the Atlantic thermohaline circulation. Nonlinear Analysis: Real World Applications 5, 501–518.

Spencer, R. W., 1993. Global oceanic precipitation from the MSU during 1979–91 and comparisons to other climatologies. J. Climate 6, 1301–1326.

Stössel, A., 1992. Sensitivity of Southern Ocean sea-ice simulations to different atmospheric forcing algorithms. Tellus 44A, 395–413.

Thorndike, A. S., Rothrock, D. A., Maykut, G. A., Colony, R., 1975. The thickness distribution of sea ice. J. Geophys. Res. 80, 4501–4513.

Untersteiner, N., 1964. Calculations of temperature regime and heat budget of sea ice in the Central Arctic. J. Geophys. Res. 69, 4755–4766.

Zhu, C., Byrd, R. H., Lu, P., Nocedal, J., 1994. LBFGS-B: Fortran subroutines for large scale bound constrained optimization. Tech. Rep. NAM-11, EECS,

Northwestern University.